The influence of metal nanoparticles ac synthesis conditions on the alumina template properties

Arūnas Jagminas

Institute of Chemistry,
A. Goštauto 9,
LT-2600 Vilnius, Lithuania
E-mail: jagmin@ktl.mii.lt

The influence of ac electrolysis conditions in various metal salt solutions on the alumina template parameters RC_0 and properties has been studied using experimental Lissajou's figures, anodic stripping and cathodic sweep voltammetry. As expected, the growth of the metallic nanoparticles within the alumina pores proceeds simultaneously with further Al substrate anodizing or Al oxide re-anodizing depending on the ac voltage applied. However, the results obtained have shown that these processes proceed at different ratios (that is, the thickness of the alumina barrier oxide layer in nm per one volt) depending also on the composition of the aqueous solutions used. Furthermore, variations of the alumina template parameters RC_0 during nanoparticle growth as voltammetric responses indirectly imply changes in the electrochemical properties of the alumina barrier oxide layer.

Key words: alumina template properties, Cu, Sn, Co nanoparticles, ac electrolysis, voltammetric responses

INTRODUCTION

During the last decade, fabrication of nano-scale arrays of metals [1–3], oxides [4, 5], semiconductors [6–9], conductive polymers [10], carbon [11], and other compounds [12, 13] within self-organized high-ordered microporous and mesoporous templates has become quite popular in various fields of chemistry and physics due to a wide application of these arrays in novel magnetic and electroluminescence displays, thermoelectric and opto-electronic devices as quantum dots, wires, or wells [3, 14, 15], catalysts [4, 16], sensors [17], two-dimensional photonic crystals [18, 19], and surface enhanced Raman scattering structures [20].

Porous anodic oxide films of aluminium formed in aqueous solutions of sulfuric, oxalic, or phosphoric acids are typical examples of self-organized three-dimensional nano-channel structures. These films, known as alumina, exhibit a packed framework of columnar hexagonal cells with central, cylindrical, uniformly sized pores, ranging from a few to about 200 nm in diameter [21, 22]. The cell size of alumina linearly depends on the applied anodizing voltage with a slope from 2.7 to 2.25 nm V^{-1} depending on the composition of the solution used [23–25]. The mesoporous layer is separated from the metal phase by a thin, mainly amorphous barrier oxide layer, impressed upon the aluminium surface as a close-packed array of hemispherical cavities [26]. During alumina growth by field-assisted transport of Al^{+3} and O^{-2}/OH^{-} ions, electrolyte species also migrate into the contaminated region of the barrier oxide layer [27] and incorporate into the alumina either directly or with a following transformation leading to the formation of Al_2O_{3-x} β $(An^{-y})_z$ γ H_2O [28]. Due to excellent thermal stability, easy handling, and the low absorption coefficient, the alumina frameworks have recently been used as templates in the formation of nanostructured materials. Besides, in the last few years high-ordered alumina have been obtained by anodizing annealed, high purity and smooth aluminium surface under appropriate conditions in sulfuric [29], oxalic [30] and phosphoric [22, 24] acid solutions by means of two-step anodizing [31], or pre-patterning of the aluminum surface before the template growth [32, 33], substantially increasing quantum effects of the composite template-wire material.

Due to rectifying properties of alumina the barrier oxide layer, an alternating current, ac, has been for a long time used for deposition of metallic and semimetallic particles commencing from the bottom of alumina pores. Although this method has been claimed as being ideal, the growth rate of particles at constant ac voltage usually gradually decreases and finally the columns stop growing [34], leaving the pores of the alumina template not fully and unevenly filled. The reasons for such behavior are not yet clear. Thus, in the meantime there is a

strong interest in fundamental studies of the behavior of alumina template and especially of the behavior of alumina barrier oxide layer during ac electrolysis.

The aim of the current work was to determine changes of alumina template resistance, capacitance and electrochemical properties with subsequent ac electrolysis in solutions of copper, tin and cobalt salts.

EXPERIMENTAL

A 99.5% pure aluminum foil containing Fe 0.24, Si 0.2, Cu 0.03, Zn 0.02, and Ti 0.01% (by weight) was used in this study. The surface of Al specimen was etched in a hot 1.5 M NaOH solution, rinsed with water, neutralized in 1.5 M HNO_3, carefully rinsed again and air-dried. The specimens were anodized at dc voltage, U_a, equal to 15 V in the stirred 1.53 M (15%) sulfuric acid solution at 18 ± 0.2 °C for 34 min. Such procedure makes it possible to obtain 10 μm thick porous anodic oxide film containing a 15 nm thick barrier oxide layer at the metal|oxide interface and a mesoporous oxide layer with cells about 37.5 nm in diameter [26]. According to [28], the $Al_2O_{2.81}(SO_4)_{0.19}$ 0.38 H_2O framework is formed. After formation, the alumina was carefully rinsed with distilled water for about 2 min and transferred into the solution for deposition of metal particles into the template nanoholes. Sine wave bias of 50 Hz frequency at a constant peak voltage value, U_p, ranging from 6 to 25 V (rms) was used for deposition of copper, tin, or cobalt particles. The composition of the solutions used is listed in Table. Two graphite rods were used as auxiliary electrodes. Ac treatments were performed at 20 ± 0.5 °C for up to 10 min.

Table. **Composition of the solutions used for deposition of metallic particles into alumina template pores**

№	Composition	Concentration, M	pH
A	$CuSO_4$ 5 H_2O	0.1	
	$MgSO_4$ 6 H_2O	0.025	4.0
	H_2SO_4	to adjust the pH	
B	$CuSO_4$ 5 H_2O	0.1	
	$MgSO_4$ 6 H_2O	0.05	1.5
	H_2SO_4	to adjust the pH	
C	$Cu(CH_3COO)_2$ H_2O	0.25	
	H_3BO_3	0.24	
	CH_3COOH	to adjust the pH	4.8
D	$CuSO_4$ 5 H_2O	0.2	
	$N(C_2H_4OH)_3$	0.66	7.0
	H_2SO_4	to adjust the pH	
E	$SnSO_4$	0.05	
	Tartaric acid, $C_4H_6O_6$	0.05	1.1
	Hydrazine sulfate	0.05	
	H_2SO_4	to adjust the pH	
F	$CoSO_4$ 7 H_2O	0.15	
	$MgSO_4$ 6 H_2O	0.1	5.5
	H_3BO_3	0.5	
	$N(C_2H_4OH)_3$	to adjust the pH	

The experimental cyclic current–voltage dependencies, *J–U*, shown in Fig. 1 and known as Lissajou's figures, LF, served as a basis for estimation of the resistance, *R*, and capacitance, C_0, of the alumina matrix. For *R* and C_0 calculations theoretical LFs in line with experimental ones (Fig. 1) were simulated using the methodology and equations derived for the equivalent circuit (EC) of parallel connected capacitance with a two-terminal network (TTN) that were reported elsewhere [35] and can be summarized as follows:

$$\frac{\partial U}{\partial t} = \begin{cases} \dfrac{U_p \sin\omega t / R_u - U(1/R_u + 1/R)}{C_0(1+VU^2)} & \text{for } U_T \le U \le U_D, \text{if } \partial U/\partial t < 0, \text{and} \\ & \text{for } U_H \le U \le U_D, \text{if } \partial U/\partial t > 0, \\ \dfrac{U_p \sin\omega t / R_u - U/R_u - J_2}{C_0(1+VU^2)} & \text{for } U < U_T, \text{if } \partial U/\partial t > 0, \\ \dfrac{U_p \sin\omega t / R_u - U/R_u - J_3}{C_0(1+VU^2)} & \text{for } U > U_D, \\ \dfrac{U_p \sin\omega t / R_u - U/R_u - J_4}{C_0(1+VU^2)} & \text{for } U < U_H, \text{if } \partial U/\partial t > 0. \end{cases} \quad 1)$$

U_p is the ac peak voltage, ω is the current frequency, C_0 is the capacitance of alumina at U = 0 V, R

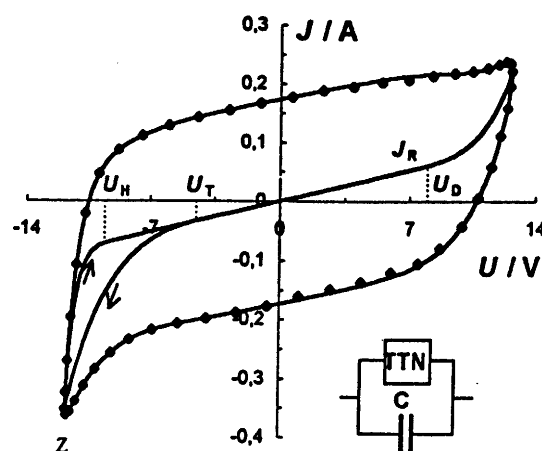

Fig. 1. Experimental Lissajou's figure of copper ac deposition process from solution **B** (Table) at the end of 60 s (points) and calculated one (line) using an equivalent circuit of the capacitance, *C*, and of a two-terminal network (TTN) in parallel with the volt-ampere characteristic of TTN, J_R. R = 6.65 kΩ cm^2, C_0 = 0.82 μF cm^{-2}, U_p = 14.07 V, B = = –0.39 V^{-1}, U_T = –4.48 V, V = 0.0025 V^{-2}, R_u = 6.4 Ω, E = = 0.545 V^{-1}, U_D = 7.97 V, U_H = –9.58 V

is the ohmic resistance of mesoporous alumina, corresponding to the resistance of TTN in a linear part of its volt-ampere characteristic signed as J_R in Fig. 1. R_u is the ohmic resistance of the external circuit. B, V, and E are freely adjustable parameters used to fit the experimental data. U_T, U_D, U_H correspond to the ac voltage U values shown in Fig. 1. The current values J_2, J_3 and J_4 are defined as:

$$J_2 = \frac{e^{B(U-U_T)} - 1 + BU_T}{RB}, \quad (2)$$

$$J_3 = \frac{e^{E(U-U_D)} - 1 + EU_D}{RE}, \quad (3)$$

$$J_4 = \frac{e^{H(U-U_H)} - 1 + HU_H}{RH}. \quad (4)$$

They describe the current flowing within distinct ac voltage ranges in accordance with the volt-ampere characteristic of TTN. The parameter H was obtained from the requirement of current continuity in the Z point by solving the transcendental equation:

$$\frac{e^{H(U_Z-U_H)} - 1 + HU_H}{H} = \frac{e^{B(U_Z-U_T)} - 1 + BU_T}{B}, \quad (5)$$

where U_Z is the voltage value at the Z point.

To investigate the changes within the alumina barrier oxide layer during ac deposition of metallic particles into the pore channels, the electrochemical behavior of alumina template was studied in the 0.1 M $MgSO_4$ solution (pH 2.0) using potential sweep voltammetry. Experiments were performed in a three-electrode one-compartment glass cell, with a carbon rod auxiliary electrode and a Ag|AgCl, KCl (sat.) reference electrode. To record the electrochemical signals, a PI 50–1.1 potentiostat equipped with a PR-8 programmer and a PC was employed. The voltammograms were recorded between 0 and –17 V at the potential sweep rate, ν, equal to 0.2 V s^{-1} at 20 ± ± 0.2 °C.

To avoid influence of the metallic particles on the electrochemical behavior of the alumina template, the deposits were dissolved immediately after their deposition by soaking the matrix in a H_2O–H_2SO_4–H_2O_2 (1:1:0.01) solution at ambient temperature for 3 min.

In accordance with [36], anodic stripping of porous alumina was performed in the solution of 0.1 M H_2SO_4 by potential sweep at a rate of 0.1 V s^{-1} from 0 to 27 V.

The amount of copper deposited within the alumina template was determined spectrophotometrically after a complete dissolution of Cu in a HNO_3–H_2O (1:2) solution according to the procedure described in detail previously [5].

All solutions were prepared using triply distilled water, high-grade acids and chemical grade salts purchased from Aldrich and used as received. Only triethanolamine was purified by distillation at 200 °C and reduced pressure.

RESULTS AND DISCUSSION

Alumina template R and C_0 variations

The conditions of electrochemical deposition of different nanoparticles at the bottom of U-shaped alumina template nanotubes and at the plane surface of conductors are quite different. Firstly, a high impedance of the barrier oxide layer, which developes at the bottom of each nanopore, requires much higher polarization for the discharge of metal ions [37]. Secondly, as can be seen from Lissajou's figures (Fig. 2), the alumina barrier oxide layer, behaving as a n-i-p semiconductor [26], rectifying the alternating current and showing the features of one-polar conductor [38] was found to transform its properties during ac electrolysis. Variations in the resistance, R, and capacitance, C_0, of the alumina template observed in the acidic solutions of copper salt during ac electrolysis, were calculated from the experimental LFs and are shown in Fig. 3. It is interesting to focus attention on these variations with ac electrolysis duration, t, showing quicker changes in the template parameters at the beginning of the process, rather than on dependence of these changes on the ac voltage. As one can see from curves 2 in Figs. 3a and 3b, the resistance of the alumina template at ac $U_p > U_a$ sharply increases, whereas C_0 decreases with t at the beginning of electrolysis, implying the further growth of the alumina barrier oxide layer. This process is completed in about 20 to 30 s after formation of a thicker barrier oxide layer. The further decrease in R and increase in C_0 may be explained only by an increase in electroconductivity of the alumina barrier oxide layer due to interaction with the solution species and/or with the products of ac electrolysis. It is well known [39, 40] that the barrier oxide layer absorbs easily the positively charged species at a certain depth at the oxide¦solution interface due to the negative volume charge of the oxide surface. On the other hand, the specific resistance and dielectric constant of the metal oxides, which determine the conductivity, strongly depend on their hydration degree. Moreover, a minor quantity of protons is needed to increase significantly the conductivity of metal oxides [41]. Taking into account what was said above, it may be supposed that the decrease in the alumina resistan-

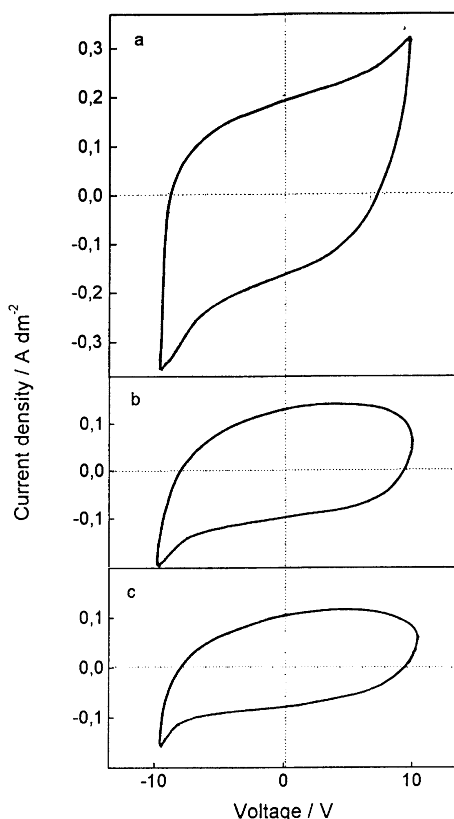

Fig. 2. *U–I* dependencies (Lissajou's figures, LFs) obtained for the alumina template during ac deposition of copper from solution **B** (Table) at the end of 5 (a), 60 (b) and 300 s (c) electrolysis at U_p 11 V

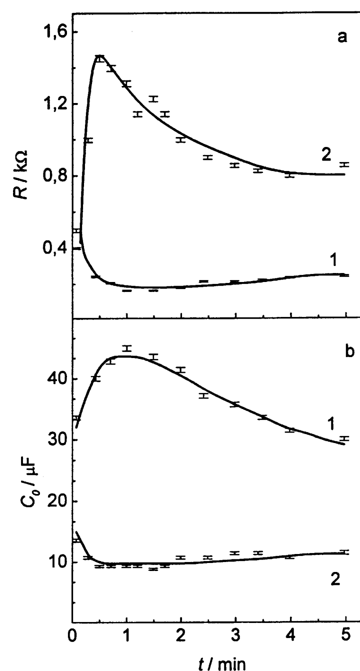

Fig. 3. Variations of the resistance, *R*, (*a*) and capacitance, C_0, (*b*) of the alumina template with ac electrolysis time, *t*, in the acidic Cu(II) solution **B** (Table) at U_p 8.5 V (1) and 22.5 V (2) calculated from the experimental LFs. The geometric surface of specimens was 50 cm^2

ce during ac electrolysis is related to hydration of the barrier oxide layer.

The calculations of *R* give an about 25 kΩ cm^2 value for the alumina template at the beginning of the first 5 s of ac electrolysis in the acidic Cu(II) solution (Fig. 3a). This value, however, is significantly lower than the resistance of the fresh mesoporous template measured in the 0.6 M solution of NaCl where at least 130 kΩ cm^2 resistance was estimated for the barrier oxide layer [42]. Therefore, it is reasonable to assume that the conductivity of the alumina barrier oxide layer increases sharply just in the first seconds of the ac treatment and that *R* and C_0 calculated from the experimental LF after 5 s electrolysis denote the resistance and capacity of partly changed alumina.

R decreases but C_0 increases with *t* at $U_p < U_a$ at the onset of the process (curves 1 in Fig. 3), which, in agreement with previously reported evidence [42], is indicative of a decrease in the alumina barrier oxide layer thickness due to re-anodizing effects or an increase in the conductivity of the barrier layer due to hydration effect. It is worth noting that the product RC_0 is considered to be constant in the case of development of uniform layers [42]. However, this is not valid in the case of the solutions used, since RC_0 value as a rule decreases with

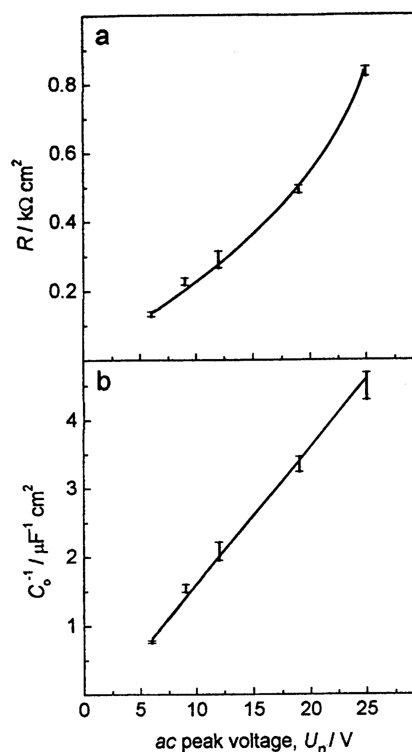

Fig. 4. Variations of alumina template resistance, *R*, (*a*) and capacitance, C_0^{-1}, (*b*) with ac U_p at the end of 300 s electrolysis in $CuSO_4$ + $MgSO_4$ (solution B)

t. The observed phenomena imply that variations in the alumina template parameters R and C_0 during deposition of metallic nanoparticles may be attributed to the changes in the barrier oxide layer thickness and properties.

The variations in mesoporous alumina resistance and capacitance $1/C_0$ with the ac voltage U_p in the acidic $CuSO_4$ + $MgSO_4$ solution (composition **B**) are depicted in Fig. 4. It should be noted that linear relations of $1/C_0$ *versus* $U_{a,fin}$ are characteristic of the alumina frameworks due to a direct dependency of the thickness of the alumina barrier oxide layer, δ_b, on the Al anodizing voltage [26, 43]. Therefore, the linear dependence of $1/C_0$ versus U_p obtained during copper ac deposition into the alumina pores (Fig. 4b) may be explained by a linear increase in δ_b with increasing U_p. On the other hand, the nonlinear plot R *versus* U_p can be explained partly by an increase in the height of copper nanowires deposited within the alumina pores and in their resistance with increasing U_p.

Anodic stripping voltammetry

The changes occurring within the alumina during ac deposition of tin, copper and cobalt particles were also supported by the behavior of the alumina template during subsequent dissolution of deposited metal particles by anodic stripping voltammetry in the sulfuric acid solution. These dependencies reflecting electrochemical responses of dissolution of nanoparticles incorporated into the alumina pores have been proposed earlier to determine the amounts of species existing in both oxide and metallic states [36]. Besides, since this process begins at the potential $E_s°$, which is strongly related to the alumina barrier oxide layer properties, arising from the alumina history we found the anodic stripping to be handy to verify the changes occurring in the alumina template. The plots of the current density, *i*, *versus* the stripping potential, E_s, obtained for the alumina template containing copper particles deposited from different solutions are shown in Fig. 5. One can see that the potential $E_s°$ at which the current appears in voltammograms depends on the composition of copper solution used for ac filling of alumina pores, although conditions of the template growth and ac electrolysis remained the same. A decrease in $E_s°$ with acidity of the Cu(II) solution indicates that changes in the barrier oxide layer properties during copper deposition are dependent on pH of the solution. The potential $E_s°$ was found to be also strongly dependent on the ac voltage used for deposition of the metal particles. As shown in Fig. 6, the plots of $E_s°$ *versus* U_p actually contain two different linear regions in the ac U_p range under investigation with

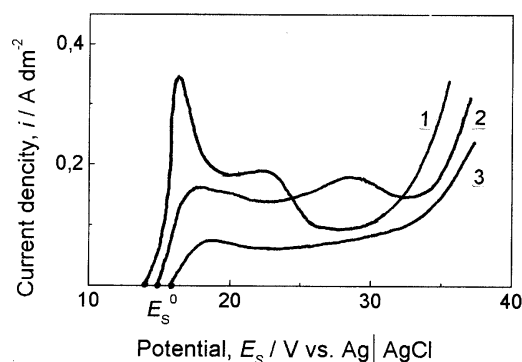

Fig. 5. Anodic stripping voltammograms in 0.1 M H_2SO_4 solution obtained at ν 0.1 V s^{-1} for the alumina template partially filled with copper particles from solutions **B** (1), **C** (2), and **D** (3) by ac electrolysis at U_p 19 V for 180 s.

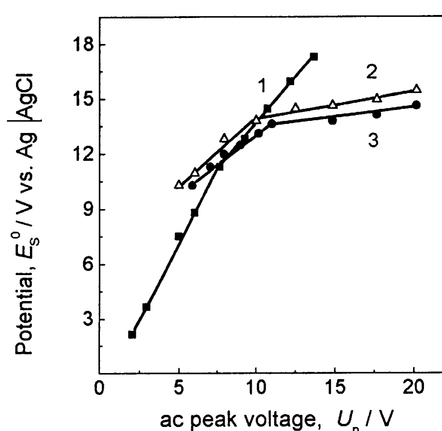

Fig. 6. Dependencies of the anodic stripping potential at which appreciable current of the copper dissolution from the alumina template appears, $E_s°$, on the ac voltage amplitude, U_p, used for copper deposition from solution: **A** (1), **B** (3) and **C** (2). ν 0.1 V s^{-1}

an obvious change in the slope at $U_p < U_a$ depending on the pH of Cu(II) solution. In fact, the potential $E_s°$ at which the electrochemical process of dissolution of the metallic particles begins, denotes the lowest value of anodic potential drop, which could be treated as an activation potential required to transfer charges through the alumina barrier oxide layer. Thus, the different slopes of the $E_s° - U_p$ plots might be indicative of the fact that the changes occurring in the barrier oxide layer during ac electrolysis (thinning, further growth and changes in properties) depend on the ac voltage applied.

Electrochemical responses of Al|alumina|$MgSO_4$ electrode

To ascertain the ac voltage regions of the alumina barrier oxide layer thickening or thinning, the behavior of the alumina template treated under various ac electrolysis conditions in copper, tin and cobalt

containing solutions was studied in 0.1 M $MgSO_4$ supporting electrolyte by potential sweep voltammetry. In agreement with previous observations [44], it may be assumed that only one cathodic wave related to hydrogen evolution is observed in this solution with a sharp current peak at the potential E_p. As shown in Fig. 7, the E_p linearly depends on the alumina template growth voltage at the end of the process, $U_{a,fin}$. Moreover, the potential at which an appreciable current of hydrogen ion reduction appears, E_{H^+/H_2}, is also linearly dependent on $U_{a,fin}$ (dashed line and the inset in Fig. 8). These results may be understood if we assume that both E_p and E_{H^+/H_2} are in a linear relation with the thickness of the alumina barrier oxide layer which has been appointed being equal to approximately 10 Å per volt for sulfuric anodizing solutions (see [26], p. 369 and references therein).

The voltammograms recorded in $MgSO_4$ solution using the alumina template that was pretreated by ac electrolysis in the metal salt solutions are similar to those shown in Fig. 7, provided that the metal particles were removed from the template by chemical dissolution. The dissolution (up to 15 min) procedure of the metallic particles in the solution containing H_2O-H_2SO_4-H_2O_2 (1:1:0.01) was found to have noticeable influence on the potential E_{H^+/H_2} and E_p at a 99% confidence level. In contrast, both E_p and E_{H^+/H_2} values for the Al|alumina|$MgSO_4$ electrode after deposition and dissolution of metallic particles were found to be strongly dependent on the ac voltage applied. A typical example of such data is shown in Fig. 8. These results show that the

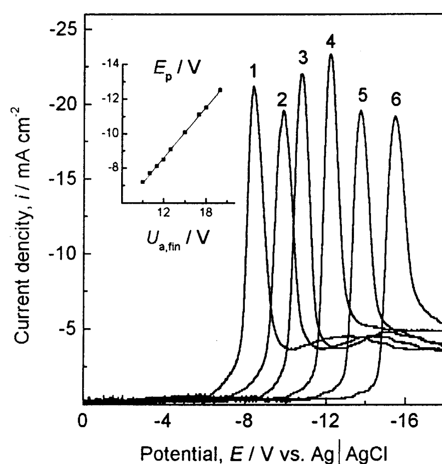

Fig. 7. Voltammograms for the Al|alumina|0.1 M $MgSO_4$ electrode at ν 0.3 V s^{-1} on the alumina re-anodizing voltage, $U_{a,fin}$: 9 (1); 11 (2); 13 (3); 15 (4); 18 (5) and 21 V (6) for 3 min. In the inset: variation of peak potential, E_p, *versus* $U_{a,fin}$

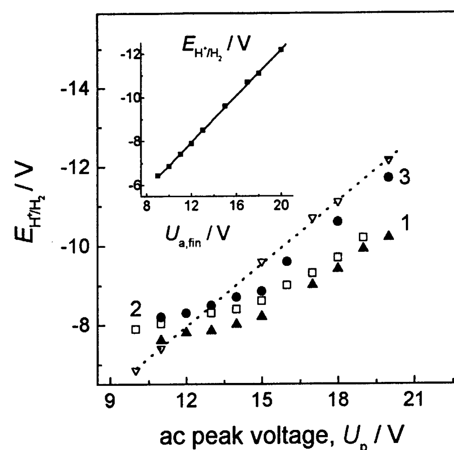

Fig. 8. Dependencies of the potential of the onset of hydrogen evolution, E_{H^+/H_2}, for same as in Fig. 6 electrode with mesoporous alumina formed at $U_a = U_{a,fin}$ = 15 V on the ac peak voltage of deposition of cobalt (1), copper (2) and tin (3) particles into the template pores from solutions **F**, **B** and **E**, respectively. Voltammetric measurements were performed at ν 0.3 V s^{-1} after complete dissolution of metallic deposits. The dashed line and the inset represent the potential E_{H^+/H_2} *versus* $U_{a,fin}$

alumina barrier oxide layer undergoes transformation during deposition of Cu, Sn, or Co within the alumina pores in an entire ac voltage range under investigation. Moreover, two regions with different slopes are clearly seen on the linear dependencies of E_{H^+/H_2} *versus* U_p at $U_p > U_a$ and at $U_p < U_a$, respectively. This implies that further aluminum anodizing performed at $U_p > U_a$ or re-anodizing at $U_p < U_a$ proceeds at different ratio, α. A comparison of the $E_{H^+/H_2} - U_p$ plots for different metal salt solutions with a linear dependency $E_{H^+/H_2} - U_{a,fin}$ clearly shows that the changes within the barrier oxide layer during ac treatment differ from those occurring in the sulfuric acid anodizing bath after U_a changes. Assuming that α = 10 Å/V for sulfuric anodizing solutions [26], the calculations for Cu(II) and Co(II) solutions give α values of about 10.2 and 8.85 Å/V, respectively. However, this is doubtful, especially for slightly acidic Co(II) solutions, where α must approach significantly higher values in the range 12 to 14 Å/V [26]. Therefore, the results obtained show that the alumina barrier oxide layer affects not only the thickness depending on the ac voltage applied, but also the properties due to interaction with the solution species.

CONCLUSIONS

The influence of ac electrolysis conditions in various metal salt solutions on the alumina template parameters RC_0 and properties has been studied using

experimental Lissajou's figures, anodic stripping and cathodic sweep voltammetry. As expected, the growth of the metallic nanoparticles within the alumina pores proceeds simultaneously with the further Al substrate anodizing or Al oxide re-anodizing depending on the ac voltage applied. However, the results obtained have shown that these processes proceed at different ratios (that is, the thickness of the alumina barrier oxide layer in nm per one volt) depending also on the composition of the aqueous solutions used. Furthermore, variations of the alumina template parameters RC_0 during nanoparticle growth as the behaviour of anodized Al electrode during subsequent voltammetric treatments indirectly imply changes in the electrochemical properties of the alumina barrier oxide layer.

Received 4 August 2003
Accepted 19 August 2003

References

1. G. H. Pontifex, P. Zhang, Z. Wang, T. L. Haslett, D. Al-Mawlawi and M. Moskovits, *J. Phys. Chem*., **95**, 9989 (1991).
2. C. K. Preston and M. Moskovits, *J. Phys. Chem*., **97**, 8495 (1993).
3. G. Sauer, G. Brehm, S. Schneider, K. Nielsch, R.B. Wehrspohn, J. Choi, H. Hofmeister and U. Gösele, *J. Appl. Phys*., **91**, 3243 (2002).
4. Y. Ishikawa and Y. Matsumoto, *Electrochim. Acta*, **46**, 2819 (2001).
5. A. Jagminas, J. Kuzmarskyte and G. Niaura, *Appl. Surf. Sci*., **201**, 129 (2002).
6. J. D. Klein, R. D. Herrick, D. Palmer and M. J. Sailor, *Chem. Mater*., **5**, 902 (1993).
7. D. Routkevitch, A. A. Tager, J. Haruyama, D. Al-Mawlawi, M. Moskovits and J. M. Xu, *IEEE Trans. Electron Dev*., **43**, 1646 (1996).
8. D. Routkevitch, T. Bigioni, M. Moskovits and J. M. Xu, *J. Phys. Chem*., **100**, 14037 (1996).
9. D. Xu, Y. Xu, D. Chen, G. Guo, L. Gui and Y. Tang, *Adv. Mater*., **12**, 520 (2000).
10. R. V. Parthasarathy and R. C. Martin, *Nature*, **369**, 298 (1994).
11. J. S. Suh and J. S. Lee, *Appl. Phys. Lett*., **75**, 2047 (1999).
12. P. R. Evans, G. Yi and W. Schwarzacher, *Appl. Phys. Lett*., **76**, 481 (2000).
13. M. El-Kouedi and C. A. Foss, Jr., *J. Phys. Chem*., **B104**, 4031 (2000).
14. N. Kouklin, S. Bandyopadhyay, S. Tereshin, A. Varfolomeev and D. Zaretsky, *Appl. Phys. Lett*., **45**, 315 (2000).
15. H. W. Hillhouse and M. T. Tuominen, *Micropor. Mesopor. Mater*., **47**, 39 (2001).
16. G. Patermarakis and N. Nicolopoulos, *J. Catal*., **187**, 311 (1999).
17. A. M. Youssef and E. A. El-Sharkawy, *Coll. Surf*., **A138**, 21 (1998).
18. H. Masuda, M. Ohya, H. Asoh, M. Nakao, M. Nohtomi and T. Tamamura, *Jpn. J. Appl. Phys.*, **38**, L1403 (1999).
19. J. Choi, J. Schilling, K. Nielsch, R. Hillebrand, M. Reiche, R. B. Wehrspohn and U. Gösele, *Mat. Res. Soc. Symp. Proc*., **722**, L 5.2.1 (2002).
20. J. S. Suh and J. S. Lee, *Chem. Phys. Lett*., **281**, 384 (1997).
21. G. E. Thompson, R. C. Furneaux, G. C. Wood, J. A. Richardson and J. S. Gode, *Nature*, **272**, 433 (1978).
22. H. Masuda, K. Yada and A. Osaka, *Jpn. J. Appl. Phys*., **37**, L1340 (1998).
23. K. Ebihara, T. Takahashi and M. Nagayama, *J. Met. Fin. Soc. Jpn*., **34**, 548 (1983).
24. A.-P. Li, F. Müller, A. Birner, K. Nielsch and U. Gösele, *J. Appl. Phys*., **84**, 6023 (1998)
25. A. Jagminas, D. Bigeliene, I. Mikulskas and R. Tamošiunas, *J. Cryst. Grow*., **233**, 591 (2001).
26. J. W. Diggle, T. C. Downie and C. W. Goulding, *Chem. Rev*., **69**, 365 (1969).
27. G. C. Wood, P. Skeldon, G. E. Thompson and K. Shimizu, *J. Electrochem. Soc*., **143**, 74 (1996).
28. Y. Fukuda, T. Fukushima and M. Nagayama, *J. Met. Fin. Soc. Jpn*., **35**, 513 (1984).
29. H. Masuda, F. Hasegawa and S. Ono, *J. Electrochem. Soc*., **144**, L127 (1997).
30. H. Masuda and K. Fukuda, *Science*, **268,** 1466 (1995).
31. A. P. Li, F. Müller, A. Birner, K. Nielsch and U. Gösele, *Adv. Mater*., **11**, 483 (1999).
32. H. Masuda, H. Asoh, M. Watanabe, K. Nishio, M. Nakao and T. Tamamura, *Adv. Mater*., **13**, 189 (2001).
33. I. Mikulskas, S. Juodkazis, R. Tamošiūnas and J. G. Dumas, *Adv. Mater*., **13**, 1574 (2001).
34. M. Saito, M. Kirihara, T. Toniguchi and M. Miyagi, *Appl. Phys. Lett*., **55**, 607 (1989).
35. A. Jagminas and J. Reklaitis, *Trans. IMF*, **81**, 98 (2003).
36. Sh. Ishida and S. Ito, *J. Met. Fin. Soc. Jpn*., **40**, 1394 (1989).
37. V. Skominas, S. Lichusina, P. Miečinskas and A. Jagminas, *Trans. IMF*, **79**, 213 (2001).
38. Z. N. Morozov, V. L. Chudiakov and A. N. Shishkin, *Electrochimiyia*, **10**, 1075 (1974).
39. A. H. Sadek, A. K. Helmy, V. H. Sabet and Th. F. Tadros, *Electroanal. Chem*., **27**, 257 (1970).
40. C. Huang and W. Stumm, *J. Coll. Interf. Soc*., **43**, 409 (1973).
41. T. P. Hoar and J. Yahalom, *J. Electrochem. Soc*., **110**, 614 (1963).
42. J. Reklaitis and A. Jagminas, in: The investigations in the field of deposition of the metals, Ins. of Chem. and Chem. Techn., Vilnius, 1985, p. 145 (in Russ.).
43. R. C. Furneaux, G. E. Thompson and G. C. Wood, *Corr. Sci*., **18**, 853 (1978).
44. A. Jagminas, J. Giedraitiene and A. Selskis, *Chemija (Vilnius)*, **11**, 3 (2000).

A. Jagminas

METALINIŲ NANODALELIŲ ELEKTROCHEMINĖS SINTEZĖS SĄLYGŲ ĮTAKA ALUMINA MATRICOS SAVYBĖMS

Santrauka

Tirta aliuminio anodinės oksidinės matricos (alumina) varžos (R), talpos (C_0) bei elektrocheminių savybių kaita užpildant jos akutes vario, kobalto bei alavo nanodalelėmis. Nustatyta, kad oksidinės matricos R ir C_0 kitimą dėl jos barjerinio sluoksnio persitvarkymo lemia ne tik kintamosios srovės lauko stiprumas, bet ir elektrolito sudėtis. Alumina matricos elgsena anodinio bei katodinio potencialo skleidimo sąlygomis po kintamosios srovės elektrolizės taip pat pasikeičia. Katodinėse voltamperogramose atsiranda tiesinių priklausomybių $E_{H^+/H_2} - U_p$; čia E_{H^+/H_2} – H_2 skyrimosi foniniame $MgSO_4$ tirpale potencialas, U_p – kintamosios srovės amplitudė, lūžiai $U_p \approx U_a$ taškuose. Šie lūžiai žymi ne tik alumina barjerinio sluoksnio plonėjimo, kai $U_p < U_a$, ar storėjimo (Al oksido tolimesnio augimo), kai $U_p > U_a$, faktą, bet ir tai, kad šie procesai priklauso nuo metalų druskų tirpalų. Alumina matrica po jos akučių elektrocheminio užpildymo Cu, Co ar Sn dalelėmis elgiasi taip, lyg jos barjerinio sluoksnio plonėjimo ar tolimesnio augimo proporcingumo koeficientai (nm/V) būtų skirtingi. Tai rodo, kad, užpildant kintamosios srovės elektrolize alumina akutes metalinėmis dalelėmis, matricos barjeriniame sluoksnyje vyksta procesai, pakeičiantys ne tik jos RC_0, bet ir elektrochemines savybes.